IEEE Access
Multidisciplinary | Rapid Review | Open Access Journal

Received April 12, 2021, accepted April 20, 2021, date of publication April 30, 2021, date of current version May 10, 2021.

Digital Object Identifier 10.1109/ACCESS.2021.3076865

Single-Trial Decoding of Motion Direction During Visual Attention From Local Field Potential Signals

MOHAMMAD REZA NAZARI[1], ALI MOTIE NASRABADI[2], AND MOHAMMAD REZA DALIRI[3], (Member, IEEE)

[1]Department of Biomedical Engineering, Science and Research Branch, Islamic Azad University, Tehran 1477893855, Iran
[2]Department of Biomedical Engineering, Faculty of Engineering, Shahed University, Tehran 3319118651, Iran
[3]Neuroscience and Neuroengineering Research Laboratory, Biomedical Engineering Department, School of Electrical Engineering, Iran University of Science and Technology (IUST), Tehran 13114-16846, Iran

Corresponding author: Mohammad Reza Daliri (daliri@iust.ac.ir)

This work was supported by the German Primate Center–Leibniz Institute for Primate Research (DPZ).

ABSTRACT Brain-Computer Interface (BCI) based on Local Field Potential (LFP) has recently been developed to restore communication or behavioral functions. LFP provides comprehensive information, due to its stability, robustness, and reach frequency content within the cognitive process. It has been demonstrated that spatial attention can be decoded from brain activity in the visual cortical areas. However, whether motion direction can be decoded from the LFP signal in the primate visual cortex remains uninvestigated, as well as how decoding performance may be influenced by spatial attention. In this paper, these issues were examined by recording LFP from the middle temporal area (MT) of macaque, employing machine learning algorithms. The animal was trained to report a brief direction change in a target stimulus which moved in various directions during a visual attention task. It was found that the LFP-gamma power was able to provide significant information to reliably decode motion direction, compared with other frequency bands, on a single-trial basis. Moreover, the results show that spatial attention leads to enhancements in motion direction discrimination performance. The highest decoding performance was achieved in the high-gamma frequencies (60–120Hz) when targets were presented inside the receptive field in opposite directions. Using a feature selection approach, performance was improved by optimally selecting features where the highest level of participation was observed in the gamma-band. Generally, the results suggest that in the MT area, LFP signals exhibit appreciable information about visual features like motion direction, which could thus be utilized as a control signal for cognitive BCI systems.

INDEX TERMS Motion direction decoding, local field potential, brain-computer interface, spatial attention, visual area MT.

I. INTRODUCTION

Visual attention is a selective mechanism which aims to prioritize behaviorally relevant information out of all subsets of sensory stimulation. It focuses on spatial positioning (spatial attention) or target-defining features (feature-based attention) across the visual cortex [1], [2]. Visual attention as a cognitive factor plays a substantial role in the higher-order mental information processing that occurs in the brain [3], [4].

BCI technology is a computer-based system that decodes and interprets brain signals in order to control an external device for performing intention or intended behaviors in humans and non-human primates [5], [6]. One of the most important issues for developing more advanced cognitive BCI systems is access to higher cortical cognitive functions, which are considerably affected by psychological states [7], [8]. Numerous studies have suggested covert visual attention in cognitive BCI applications [9]–[11].

Various BCIs have been made operational based on invasive or noninvasive recording technologies. Among the non-invasive techniques for recording brain activity, electroencephalography (EEG) has been widely employed in BCI applications [12]–[14]. At the neuroscience and neuroengineering levels, most current knowledge on the neural

The associate editor coordinating the review of this manuscript and approving it for publication was Derek Abbott.

foundations of visual attention is based on brain activity processing, which comes from invasive electrophysiological studies in non-human primates. As invasive recording sources, single units and local field potentials are employed to extract practical features to drive BCI systems [15]–[17].

LFP is one of the brain activity aspects that provides a dynamic flow of information for cognitive processing. LFPs are low-frequency extracellular voltage fluctuations that are thought to reflect the aggregate of synaptic activities in a population of local neurons around a recording [18]. Previous studies have demonstrated that the composition of spike activity recorded changes over time, probably due to micro-motions of recording sites or the loss of neural tissue near the electrode tips. This can lead to the decline of static performance and require frequent calibration in BCI systems [16], [19]–[21]. Moreover, the procedures regarding spike processing, such as spike sorting and firing rate estimation, are time-consuming and complex. Consequently, the use of decoded information from LFP signals, due to their stability, robustness, and reach frequency content, has attracted interest in brain structure and cognitive processing studies. Thus, this type of brain activity may be presented as suitable research topics for the problem solution of spike-based BCI systems [15], [22]–[24].

The influence of visual attention on LFP signals has been reported across different cortical sensory areas of monkey [25]–[30]. Numerous studies have demonstrated that visual attention affects the modulation of neuronal processing in a variety of perceptual tasks [31]–[34]. It has been shown that spatial attention enhances the response gain of sensory neurons when the stimulus is located in the receptive field [25], [35]–[37]. In particular, switching attention into the receptive field (RF) is associated with a decrease in low-frequency oscillations, as well as an increase in high-frequency oscillations, in LFPs of the visual sensory areas [26]–[28], [38], whereas one study reported different results [29]. In contrast, feature-based attention (FBA) improves the perception of relevant stimulus features (e.g., color, motion direction, or shape), at the expense of behaviorally-irrelevant features, via modulation of the feature-selective neurons' responses throughout the visual cortex [39]–[42].

The impact of spatial attention and FBA on the response modulations of visual cortical neurons have been investigated together in a number of studies [43]–[45]. Furthermore, psychophysical studies have confirmed the interaction between spatial and feature-based attention by analyzing spike activities from lateral the intraparietal [46], V4 [47], and MT [48] areas. These results demonstrate that attention to relevant visual features located inside each neuron's RF boosts FBA gain modulations. Several studies have evaluated the feasibility of decoding information about movement goals from the LFP signals in the motor cortex [49]–[51]. Slutzky *et al.* reported that LFP signals could be used for decoding the forelimb movements of rats in the sensorimotor cortex [52]. Other studies showed that LFP signals recording from multi-cortex (i.e. the primary motor cortex, the somatosensory cortex, and the posterior parietal cortex) were utilized for decoding reaching and grasping movements [53]. Moreover, high decoding performance was obtained by combining the high-frequency LFP signals from three-cortex studies compared to single-cortex studies. These studies conclude that LFPs are more robust and durable, thus providing an accurate signal source for applications of BCIs.

Visual attention affects the frequency characteristics of LFP activities, which leads to an appropriate signal for decoding information during attention tasks. Several types of research have employed LFP signals for decoding the focus of attention during different visual tasks. For instance, the effects of visual stimulus on decoding performance during the object-detection task in the macaque inferior temporal cortex have been studied [54], [55]. Some studies have demonstrated the ability of LFP signals to decode two-position spatial attention, while LFP was recorded from the macaque MT area [56], [57]. In other studies, the possibility of predicting the allocation of covert attention has been investigated in different areas of the monkey brain: from the LFP [58]; spiking activity from the lateral prefrontal cortex [59], [60]; and the frontal eye field [61]. Similarly, decoding the focus of attention during the shape-tracking task based on electrocorticogram (ECoG) recordings has been examined [62]. Summarizing the survey mentioned above, it can be seen that the brain activity recordings in different visual cortex areas in certain frequencies contains valuable information to decode the allocation of attention or visual stimulus location. However, it remains uninvestigated as to how the motion direction-related information can be decoded from LFP signals in the primate visual cortex.

According to the above discussion, this paper aims to investigate motion direction decoding by applying the LFP signals recorded from the MT area of a monkey. For this purpose, the animal had to report a brief direction change in a target stimulus during a spatial-based visual attention task. In addition, the decoding performance of motion direction across different frequency sub-bands is examined by employing machine learning algorithms.

The results reveal that motion direction can be decoded using LFP-power on a single-trial basis across different frequency bands. Furthermore, high gamma-frequency oscillations carry substantial information about the stimulus motion direction. This is consistent with results obtained from the feature selection analysis, which has shown the largest portion of this frequency range in motion direction decoding. Noticeably, decoding performance is enhanced when the monkey's attention is directed to the stimulus direction inside the neuron's receptive field. In this study, it is suggested that the LFP signals recorded from the MT visual cortex could be utilized for cognitive information processing, such as covert attention to motion direction, in order to be offered as a control signal for cognitive BCI systems.

This paper is organized as follows. Section II briefly explains the behavioral task, LFP recording, and data pre-

processing. Section III provides the results, including evaluating LFP information content and decoding performance, based on different analyses. The discussions are provided in Section IV, and conclusions in Section V.

II. MATERIALS AND METHODS

All animal procedures in this study were conducted at the German Primate Center in Göttingen, Germany, according to all local applicable laws and regulations, and were approved by the responsible regional government office [Niedersaechsisches Landesamt fuer Verbraucherschutz und Lebensmittelsicherheit (LAVES)].

A. BEHAVIORS TASK

In this study, extracellular neuronal activities are recorded from the macaque MT area, which is a visual area largely devoted to visual motion processing. The male macaque monkey was trained to fixate on a central fixation and directed its attention to one of two coherently moving random dot patterns (RDP). The animal had to press a lever to initiate each trial while keeping the gaze on a central fixation point for 130 ms. In each trial, a cue appeared on the screen for 455 ms, showing one of the upcoming moving RDP as a relevant stimulus (target). After 325 ms, that the cue was removed, and two pairs of moving RDPs were simultaneously shown at a random time between 680–4250 ms, one located inside the recorded neuron's receptive field and the other located in the opposite visual hemifield. Both RDPs moved in the same direction in one of eight possible directions selected randomly in each trial (0–360° with steps of 45°). During this time period, one or both of the stimuli could randomly underwent a brief (130 ms) direction change. The monkey had to detect a direction change in the target RDP within a response time interval of 150–650 ms by releasing the lever to receive a reward. The direction change could also happen in the un-cued stimulus (as a distractor). Trials in which the monkey responded to such changes were ended without reward and considered errors (Fig. 1).

The behavior paradigm included two types of trials: ones where attention was focused within the receptive field; and ones where attention was diverted towards a stimulus placed outside the receptive field. The monkey correctly released the lever for the response to a target change in 86% of the trials without fixation breaks. The incorrect response to the distractor change occurred in 3% of trials. Also, the monkey terminated the trial without performing any response in 11% of trials (miss trial).

This data includes two components, single-unit activities (SUAs) and LFP signals, which were recorded from the MT area using a multichannel acquisition processor (MAP) data acquisition system (Plexon, USA) and a 5-channel Mini-Matrix driver (Thomas Recording, Germany). Signals were recorded from up to all five electrodes (with the impedance of 2 MΩ arranged linearly separated by 300 μm) simultaneously. Signals were amplified and filtered by hardware filters. Spikes and LFPs were digitized at 40 kHz and 1 kHz, respectively. Spikes were sorted using the Plexon spike sorter (Plexon, USA). The sites located in the MT were determined by direction selectivity of isolated cells and the electrode position relative to the cortex.

B. DATA ANALYSIS

In this section, the aim is to describe data preprocessing, which was carried out using MATLAB software (Mathworks, Natick MA). In an initial step, the LFP for each trial and channel was filtered by a 3rd-order Butterworth filter to remove the 50 Hz line noise implemented with zero phase-shift ('filtfilt' function in MATLAB) to prevent any phase distortion.

To investigate the information content relevant to motion direction in each frequency band, a 3rd-order Butterworth band-pass filter was used to divide the LFP frequency spectrum into the following bands: delta (1–4 Hz), theta (4–8 Hz), alpha (8–12 Hz), beta (12–30 Hz), low-gamma (30–60 Hz) and high-gamma (60–120 Hz). Then, The first and last 200 ms of the filtered LFP was dropped to avoid any possible edge effects created by filtering at both ends of the signal time segment. Therefore, the LFP signal was analyzed in the period between (200 ms to 1200 ms) after the stimuli onset.

A total of 32 sessions were recorded, but only sessions with the following conditions were included in the analyses: (I) sessions with at least two electrodes within the MT region; and (II) sessions with at least ten correctly performed trials per condition, which had eight possible directions, i.e. 0°–360° with steps of 45°. Hence, the overall numbers of selected recordings contained 20 sessions and 72 sites. The power spectral density (PSD) of each single trial can be estimated by computing the magnitude squared of the discrete Fourier transform applied to the signal. Each trial PSD is normalized by the overall PSD mean across trials from each attention condition (i.e. trials of possible direction pairs) for each site.

In this paper, decoding performance was considered on a single-trial basis from LFP signals across each sub-band. The use of artificial intelligence methods in BMI and BCI systems is gradually increasing. Classification is often an essential part of the process in many different fields, such as decoding the attentional state of the monkey. Classifiers are usually trained by applying some kind of supervised machine learning approaches, including generalized linear models, linear regression, Bayes classification, or support vector machines (SVM) [22].

In the next step, SVM [63] was applied to estimate classification accuracy using a 10 × 10-fold cross-validation method to separate the two motion directions from the LFP signal at each sub-band. The classification performance values were obtained by averaging over the folds and repetitions of the cross-validation. The statistical significance of decoding performance was assessed using a permutation test. The target labels on the observed data points were randomly shuffled. Then, classification performance was calculated as above. This was repeated 100 times for each file. Eventually, the mean and standard deviation were calculated from the

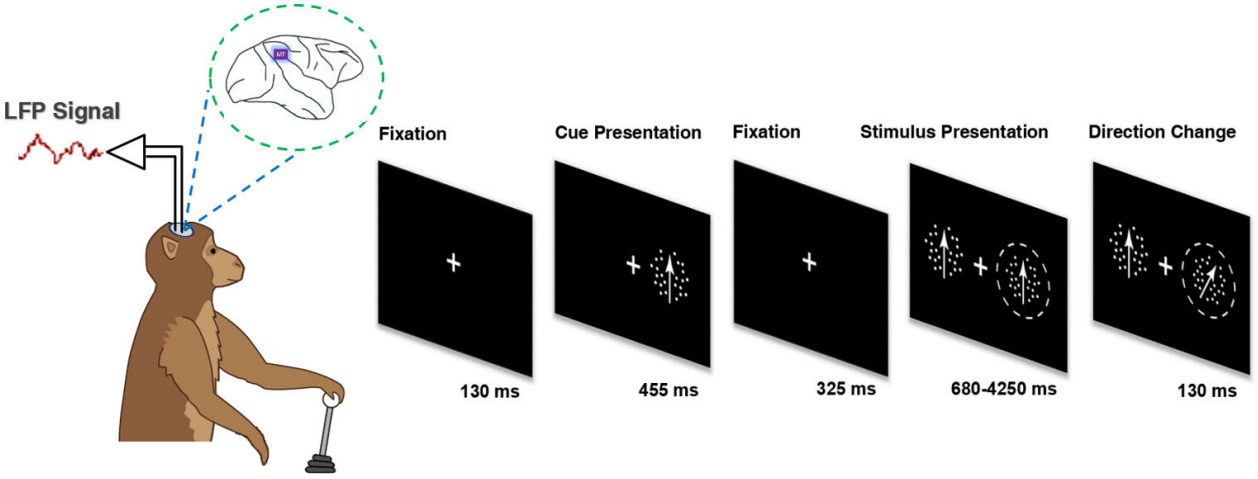

FIGURE 1. Behavioral paradigm. The monkey had to touch a lever to start the trial, while fixating the central fixation spot for 130 ms. Then, a cue appeared for 455 ms on the screen, indicating one of the upcoming relevant stimulus positions. After a blank screen period of 325 ms, two moving RDPs were shown at a random time between 680–4250 ms. During this time period, one or both of the stimuli randomly underwent a short direction change for 130ms. The monkey had to report a direction change in the target RDP within a response time interval of 150–650 ms by releasing the lever to receive a reward.

generated distribution to set the 95% confidence intervals for chance performance. In this paper, state-dependent differences were computed using a repeated-measures analysis of variance (ANOVA), followed by post-hoc Bonferroni test for multiple comparisons (Figs. 2(d), 6). Permutation test with false discovery rate (FDR) correction was employed for examining the difference of curves among sensory conditions (Fig. 3). Additionally, two-sided Wilcoxon rank-sum test was performed for computing the difference between the two conditions with FDR correction for multiple comparisons (Figs. 4, 7).

III. RESULTS

The feasibility of the motion direction decoding was evaluated based on LFP signals recorded from the MT area of a macaque monkey in a target change-detection task. During the task, the monkey had to detect a brief motion direction change in one of two moving RDPs (target stimulus) and to ignore the other one (a distracter). The RDPs could move in one of the possible eight directions (0°–360° with steps of 45°), and both had the same direction in each trial. In half of the trials, the monkey was cued to attend to the target stimulus, inside the RF, and in the other half of trials, it was cued outside the RF.

For the decoding of LFP-directional information, each trial was analyzed on a period between 200 ms to 1200 ms after stimulus onset. In this processing, there were a total of 28 possible pairs of motion directions (0° vs. 45°, 0° vs. 90°, 0° vs. 135° …270° vs. 315°), depending on the eight different target directions.

A. THE LFP DIRECTION OF MOTION INFORMATION ANALYSIS

We investigated how the difference in LFP-power changed as a function of the target direction differences. To evaluate this case, first, LFP-power was calculated in each of the eight directions during the period of 200–1200 ms after stimulus onset within the frequency range of 1–120 Hz for each trial. Then, these values were averaged across trials and sites corresponding to each direction. Second, the difference in powers of all 28 pairs of directions and across frequency bands were computed separately.

To assess the quantitative magnitude of differences, the base-10 logarithm of the ratio between the powers in two target directions was computed during all trials relevant to each direction pair. Then, these relative powers (i.e. log-ratio) were averaged across trials and recording sites. To present a smoothed outcome, the PSD and relative power were convolved with a Gaussian function ($\sigma = 2$) (Fig. 2). Examples of the LFP signal power (mean ± SEM) in a frequency range for direction 0° versus four target directions (45°, 90°, 135°, and 180°) are illustrated in Fig. 2(a). As observed, the power curves corresponding to the two directions diverge in specific frequency ranges.

Fig. 2(b) shows examples of mean relative power across frequencies for direction 0°, compared with other directions. Positive values of the average relative power indicate that the power amplitude of direction 0° is stronger than the other direction. Examples of time-frequency maps of the LFP-power differences between directions of 0° − 45° and directions of 0° − 180° are illustrated in Fig. 2(c). The plot showed clear differentiations in terms of information content between different time courses and frequency bands.

The result is evident that the difference in LFP-power in the high-gamma significantly increases compared with other sub-bands. Also, the greatest amount of direction-related information was provided in the time periods of 200-400 ms and 850-1200 ms.

To assess the effect of motion direction on LFP-power, repeated-measures ANOVA was used, followed by

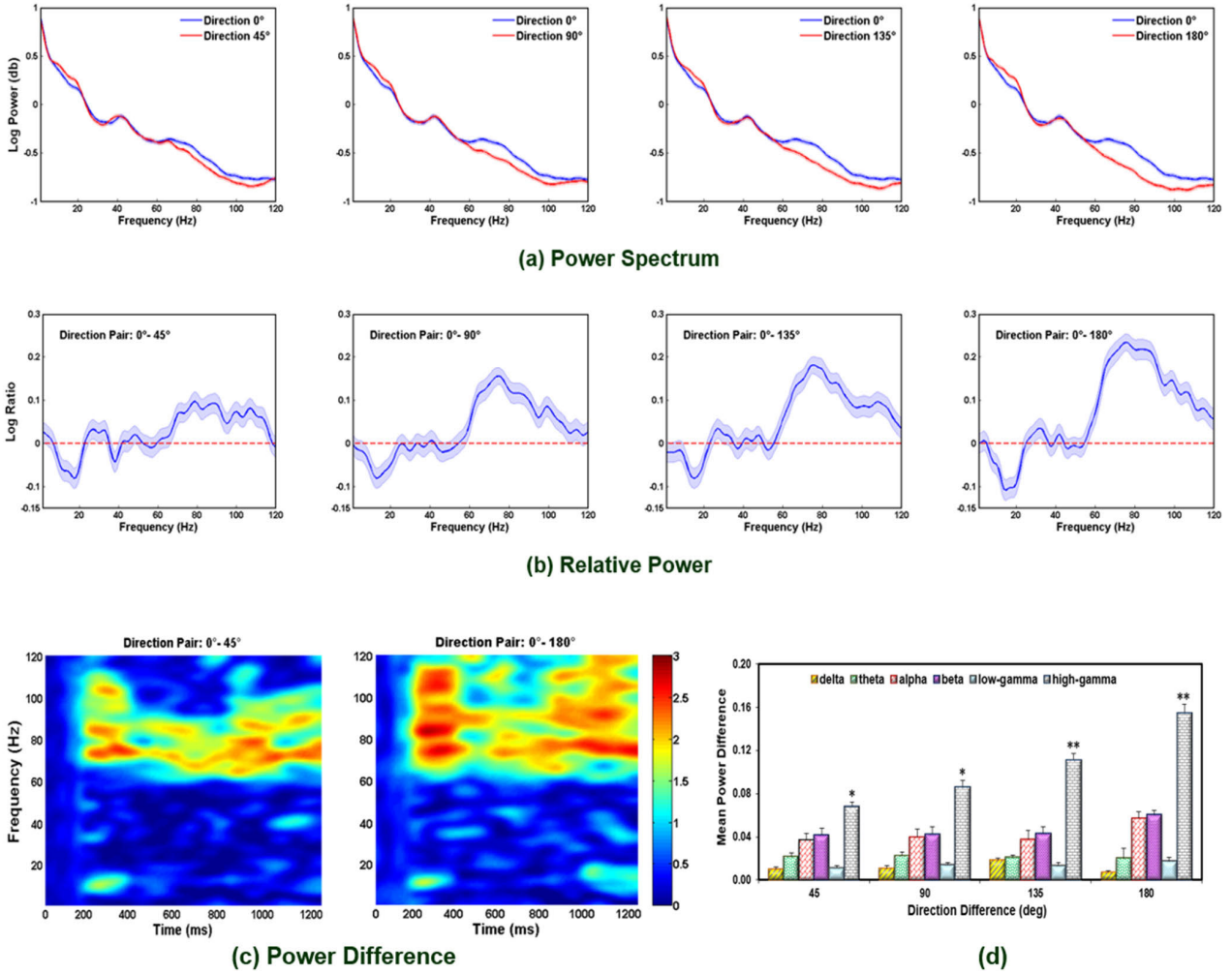

FIGURE 2. LFP analysis for the different target directions at different frequencies. a. The plots show the normalized mean LFP power for the direction 0° versus four target directions (out of 7) located inside the RF for the recording sites (n = 72). b. The mean relative power, calculated as the base-10 logarithm of the ratio between the powers in the two target stimuli. The relative power (log–ratio) was computed during trials of two directions and then averaged across trials and sites. c. Representative time-frequency maps of the LFP-power differences between directions of 0°-45°, and directions of 0° − 180°. The data were aligned to the starting point of the stimulus (t = 0 ms) and analyzed over the period of 0-1200ms. d. Mean LFP-power difference for direction differences of 45°, 90°, 135° and 180° across frequency ranges. Star indicates significant difference between frequency bands in each sensory condition (*$p < 0.05$, **$p < 0.001$, repeated measures ANOVA, with a post-hoc Bonferroni's multiple comparison test). Error bars indicate SEM.

post-hoc Bonferroni test with frequency bands (delta, …high-gamma), spatial-attention, and direction differences (45°, 90°, 135°, 180°) as subject factors (Fig. 2(d)). Quantitative analyses of power differences revealed significant main effect of direction difference ($F_{(3,699)} = 30.67, p \ll 0.0001$). Repeated-measures ANOVA also showed significant frequency bands × direction difference interaction ($F_{(15,699)} = 23.36, p \ll 0.0001$), as well as a spatial-attention × direction difference interaction effect ($F_{(3,699)} = 24.18, p \ll 0.0001$). As shown in Fig. 2(d), the difference in LFP-power in the high-gamma range significantly increases, compared with other sub-bands for all direction differences across attention conditions (repeated-measures ANOVA with post-hoc Bonferroni test).

To examine the relationship between the angular difference and difference in power, the power differences between each direction pair were computed in the gamma frequency range. The absolute value of these differences was then averaged separately across direction pairs in which the angular differences between directions pairs were 45°, 90°, 135°, and 180° (Fig. 3). It is visually evident that increasing the direction pair differences leads to significant differences in high-gamma power. According to Fig. 3, the magnitude of power differences for a 180-degree difference is significantly greater than a 45-degree difference in directions.

B. DECODING OF MOTION DIRECTION

This paper mainly focused on the discrimination of target motion direction within every possible pair of directions. To investigate which LFP frequency bands contained the maximum motion directional information, the PSD of each sub-band was computed as a feature in every single trial. Then these features were fed to an SVM classifier with an

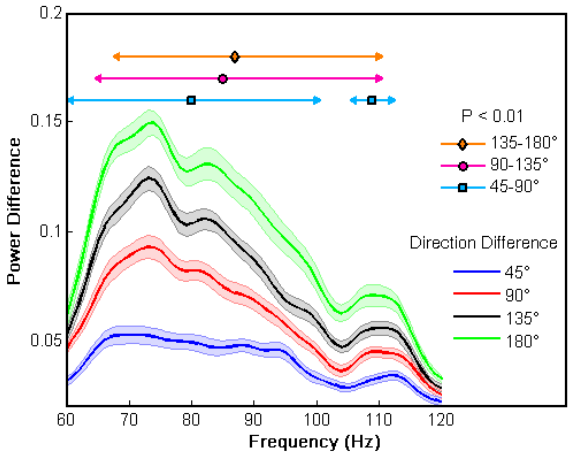

FIGURE 3. LFP-power in the direction differences configurations in the high-gamma band (60–120 Hz). The curves represent power differences as a function of direction differences. Results are shown for the various direction differences (45°-blue, 90°-red, 135°-black, and 180°-green). Colored lines on top of the traces indicate significant differences in power between conditions, 45°–90°, cyan; 90°–135°, magneta;135°–180°, orange (permutation test, FDR corrected for multiple comparisons). Error bars indicate SEM.

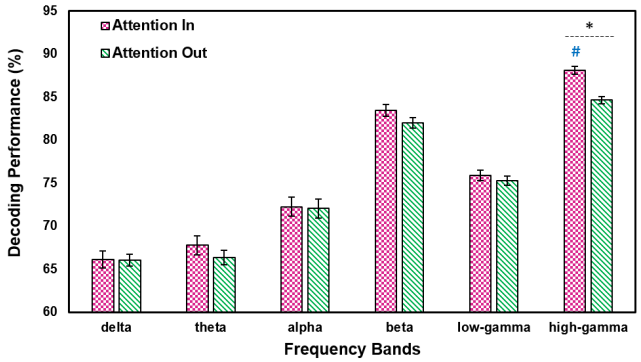

FIGURE 4. Decoding performance of motion direction in different frequency bands at each spatial attention condition. The star indicates a significant difference in decoding performance between inside the RF and outside the RF (*$p \ll 0.001$, two-sided Wilcoxon rank-sum test; #$p < 0.05$, FDR corrected for multiple comparisons). Error bars indicate SEM.

SMO solver and an RBF kernel function for motion direction decoding. First, each pair of directions was classified separately by the SVM classifier using the 10 × 10-fold cross-validation procedure. Then, the average classification accuracy in all 28 possible pairs was expressed as the decoding performance value, and this process was examined for each sub-band, and also at each target location condition (inside the RF/outside the RF).

The results indicated that the classification performance in all frequency sub-bands was significantly higher than chance level (permutation test, $p < 0.05$). It was found that the high-gamma band reached the highest performance in decoding motion direction, compared with other frequency bands (88.11% ± 2 (SD)) ($p < 0.05$, Wilcoxon rank-sum test, FDR corrected for multiple comparisons; Fig. 4). Moreover, the next highest performance was obtained in the beta and

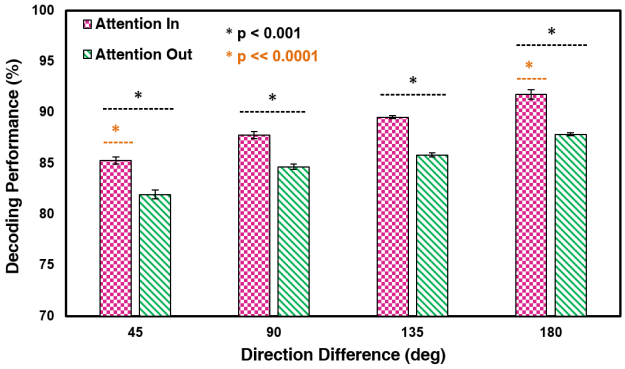

FIGURE 5. Decoding performance in the high-gamma frequency band (60–120 Hz), in direction difference configurations. Decoding accuracy was calculated for all pairs with direction differences of 45°, 90°, 135° and 180° in each behavior condition. The star denotes a significant difference in performance between conditions (two-sided Wilcoxon rank-sum test). Error bars indicate SEM.

low-gamma bands with 83.48% ± 3 (SD) and 75.88% ± 3 (SD), respectively, which were significantly smaller than the highest performance in the high-gamma band (beta & high-gamma band, $p \ll 0.0001$, low- gamma & high-gamma band, $p \ll 0.000001$, two-sided Wilcoxon rank-sum test). It is thus suggested that the high-gamma band contains valuable information for the direction of motion decoding.

To examine how spatial attention affected motion direction decoding, significant differences in decoding performance were evaluated separately between two target positions across frequency bands. It was observed that only in the high-gamma band, the direction decoding in these two position conditions differed significantly (inside RF: 88.11% ± 2 (SD), outside RF: 84.66% ± 2 (SD), $p \ll 0.001$, two-sided Wilcoxon rank-sum test) (Fig. 4). It is therefore inferred that the decoding performance of the motion direction in the high-gamma band was affected by spatial attention. Based on the obtained results, since the highest decoding performance was achieved in the high-gamma range (and only in this frequency band), the effect of location on decoding performance can be observed; decoding performance in all pairs of directions has therefore been evaluated in this sub-band. By decoding analysis in the high-gamma band, the highest and lowest performance, reached at angular differences 180° (90° vs. 270°, in RF / out RF) and 45° (0° vs. 45° in RF & 0° vs. 315° out RF), respectively. Furthermore, it was found that attention inside the RF is associated with increased decoding performance of all direction pairs in this frequency sub-band (Table 1).

To examine the effects of the direction difference on the decoding performance, all cases with direction differences of 45°, 90°, 180°, and 135° were analyzed. As expected, when the two targets had 180° direction differences, decoding performance was significantly higher than when the direction differences were 45° (inside RF: 45°-difference, 85.24% ± 2 (SD); 180°-difference, 91.74% ± 2 (SD), $p \ll 0.0001$, two-sided Wilcoxon rank-sum test). It is inferred

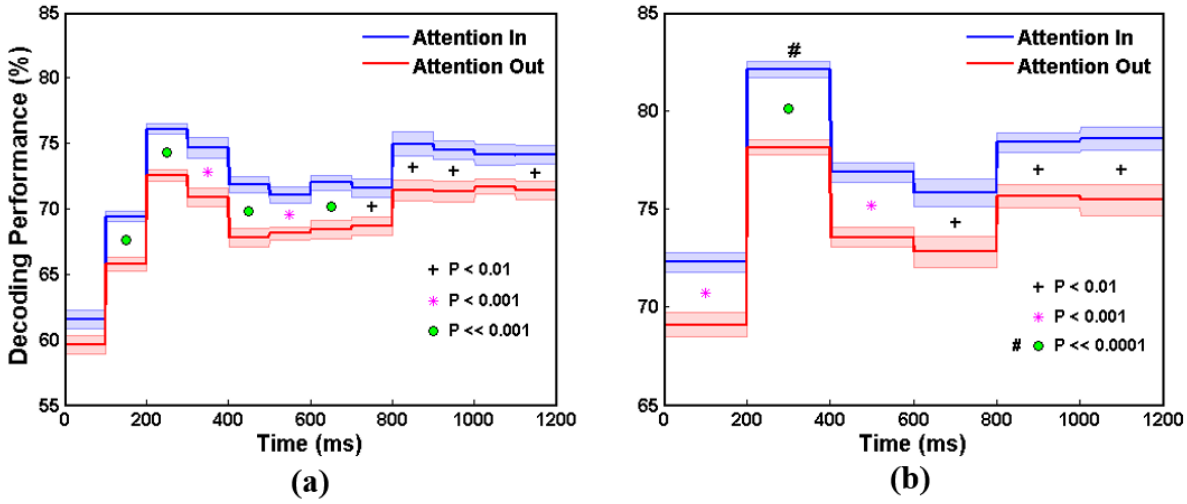

FIGURE 6. Time course of the single-trial decoding performance. The data were aligned to the onset of the stimulus (t = 0 ms) and analyzed in the period 0-1200 ms. The blue and red curves illustrate the temporal dynamics of motion direction decoding of LFP signals for attention inside the RF and attention outside the RF, respectively. Decoding accuracy was computed based on the high-gamma power for analysis windows of 100 ms (a) and 200 ms (b). "#" denotes significant differences in performance between time intervals. The solid circle, star, and plus show significant differences in performance between two attention conditions (repeated-measures ANOVA with a post-hoc Bonferroni's multiple comparison test). Error bars indicate SEM.

TABLE 1. Performance of high gamma-band power (60–120Hz), in motion direction decoding. Decoding accuracy was calculated in each possible direction pair and each spatial attention condition (Attention In, cyan; Attention Out, gray). The maximum and minimum performance values are shown in yellow and magenta boxes, respectively.

Direction	Decoding Performance (%); Attention Out							
	79.45	84.6	85.3	87.85	86.05	85	81.6	
	85.55	86.55	88.2	86.2	85.1	83.25		86.5
	85.55	87.7	85.15	84.25	82.85		85.35	88.55
	87.55	86.1	83.85	82.75		85.95	86.75	89.3
	85.4	85.1	81		86.45	86.95	89.45	91
	83.75	82.55		84.4	87.5	89.35	93.05	88.8
	82		84.95	86.9	90.15	92.65	89.55	88.55
		83.75	87.55	89.75	90.25	89.7	89.25	84.55
Direction	0°	45°	90°	135°	180°	225°	270°	315°

Decoding Performance (%) Attention In

that the greater the angular difference in the pair of directions, the higher the decoding performance (Fig. 5).

C. TIME COURSE OF DECODING PERFORMANCE

To examine the temporal evolution of decoding performance, classification accuracy was estimated using data within sliding 100 and 200 ms time windows, starting immediately from stimulus onset. In each time step, the power spectral density of the high-gamma band was calculated across trials in each direction. These PSDs are considered as features which can discriminate motion direction. Therefore, the number of extracted features was 60 for each window size. For classification, the SVM was utilized with SMO solver and RBF kernel function ($\sigma = 3$). Classification performance was obtained by averaging all accuracy values (28 possible direction pairs), calculated in both spatial positions (inside the RF / outside the RF).

To determine statistical differences between classification performances for two attention conditions across time intervals, repeated-measures ANOVA with post-hoc Bonferroni's multiple comparison test was performed. Time-course analysis showed that there was a significant main effect of time intervals (window size: 200 ms, $F_{(5,390)} = 71.80$, $p \ll 0.0001$; window size: 100 ms, $F_{(11,858)} = 95.3, p \ll 0.0001$). Post-hoc analysis indicated a significant difference in performance between two attention conditions during all time inter-

vals for 200 ms window size; for a window size of 100ms, significant differences were observed across time intervals except intervals of 0-100 ms and 1000-1100 ms (Bonferroni post-hoc test).

It was found that the lowest performance was obtained at time intervals of 0-100 ms ($p \ll 0.0001$, Bonferroni post-hoc test; Fig. 6(a)) and 0-200 ms ($p < 0.001$; Bonferroni post-hoc test; Fig. 6(b)) after the stimulus onset, for window lengths of 100 ms and 200 ms, respectively. This is probably due to the delay in MT neuronal response, since it takes time for the neuron populations to propagate the response at the extrinsic terminators [64]. In addition, performance reached its peak in the first time window, starting from 200 ms after the stimulus onset, which is evident in Fig. 6(b) ($p \ll 0.0001$, Bonferroni post-hoc test). Also, the performance almost remained constant in a time interval of 400-800 ms after the target presentation until prior to change onset. Moreover, it was observed that performance increased during the change epoch occurring about 815 ms after stimulus onset (the starting time of the change epoch varied across trials).

The results show that there was a significant difference in performance between window lengths of 700-800 and 800-900 ms ($p < 0.01$, Bonferroni post-hoc test; Fig. 6(a)), and also between the window lengths of 600-800 and 800-1000 ms ($p \ll 0.0001$, Bonferroni post-hoc test; Fig. 6(b)). This could be due to the onset of a change in stimulus direction. To compare the performance results in all windows fitting within the time interval (0-1200 ms), the maximal accuracy values were selected for each window length for two attention positions. It was observed that applying a window width of 1000 ms resulted in the highest classification performances, while shorter analysis windows led to performance reduction during the time course ($p < 0.05$, Wilcoxon rank-sum test, FDR corrected for multiple comparisons; Fig. 7). In general, for each size of the analysis window, covertly attending to the target direction inside the RF significantly enhanced decoding performance ($p \ll 0.001$, two-sided Wilcoxon rank-sum test).

D. DECODING PERFORMANCE ANALYSIS BASED ON FEATURE-RANKING METHOD

It was also examined whether the feature selection method could lead to improvements in decoding performance, and which subset of features was more informative for decoding motion direction. For this analysis, a scalar feature-ranking method based on the Wilcoxon criterion was utilized, selecting optimal informative features to increase classification accuracy.

Briefly, the PSD of the LFP signal was calculated for frequency bands ranging from 1 Hz to 120 Hz for each direction. This provided 120 components of the power spectrum, which was proposed as a classifier input for the direction of motion decoding. This feature ranking method was applied for each direction pair. To do this, all features were ranked separately according to the p-value; then, these features were fed into the SVM classifier sequentially. At each stage, the average

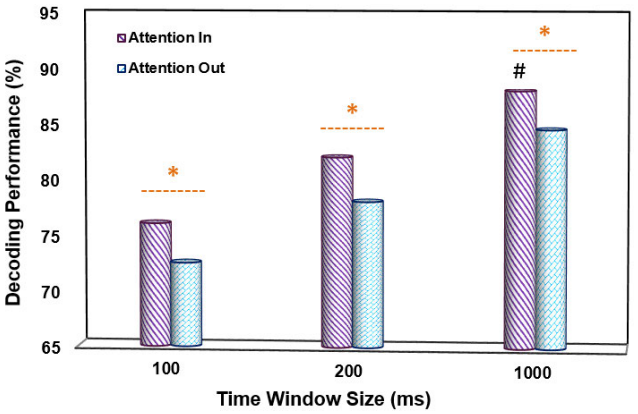

FIGURE 7. Dependence of the decoding performance on the time window size. This figure represents the maximal decoding performances for each window size. The maximum accuracies were obtained for window lengths of 100 ms, 200 ms, and 1000 ms regarding the time intervals of 200-300 ms, 200-400 ms, and 200-1200 ms, respectively. Stars denote significant differences in performance between conditions (*$p \ll 0.001$, two-sided Wilcoxon rank-sum test; #$p < 0.05$, FDR corrected for multiple comparisons). Error bars indicate.

decoding accuracy was computed by applying a 10×10-fold cross-validation procedure. Finally, according to 28 possible pairs, the classification accuracy was estimated via the average accuracy values across all direction pairs.

Fig. 8 shows the mean decoding accuracy of the Wilcoxon criterion-based feature selection algorithm for an increasing number of features across two spatial attention conditions. As seen in Fig. 8, for the target located inside and outside the RF, the numbers of selected features regarding maximum classification accuracy were 88 and 103, respectively. For attention inside the RF, performance with and without feature selection was 91.76% $\pm$ 1.7 (SD) and 87.1% $\pm$ 1.6 (SD), respectively. For Attention outside the RF, performance with and without feature selection was 87.13% $\pm$ 1.7 (SD) and 83.71% $\pm$ 1.6 (SD), respectively (Fig. 8). It is obvious that this feature selection algorithm improved the classification performance across both behavior conditions (all features & selected features: inside the RF & outside the RF, $p \ll 0.0001$, two-sided Wilcoxon rank-sum test).

In this paper, selecting a lower number of features is preferred to slightly higher improvement in performance. Therefore, the optimal trade-off between the number of selected features and classification accuracy is provided by the following equation:

$$\text{Error}_{\%1} = \left(\frac{\text{Accuracy}_{(\text{Max})} - \text{Accuracy}_{(i)}}{\text{Accuracy}_{(\text{Max})}} \right) < 0.01 \quad (1)$$

where i indicates the number of features. According to this equation, the optimal subset of features is selected when the normalized difference between the average accuracy of these selected features and the maximum average accuracy is less than 1%. Consequently, the numbers of selected features for attention inside the RF and outside the RF are 62 and 80, respectively.

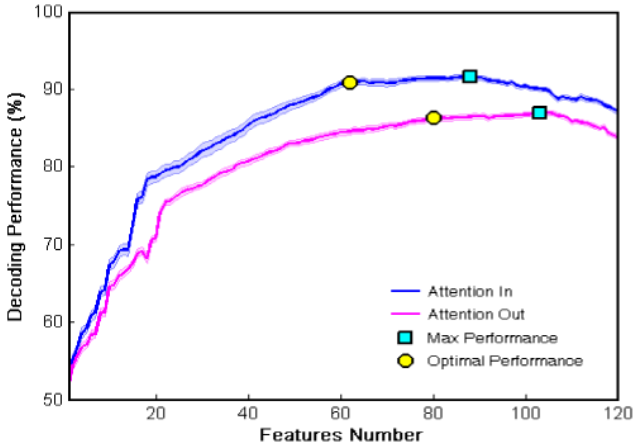

FIGURE 8. Feature selection analysis-based decoding performance. The curve illustrates the decoding accuracy as a function of selected features, with increasing number of features in two behavior conditions. The square (cyan) and the solid circle (yellow) in each graph show the maximum performance and performance value corresponding to optimally selected features, as calculated with equation (1). Error bars indicate SEM.

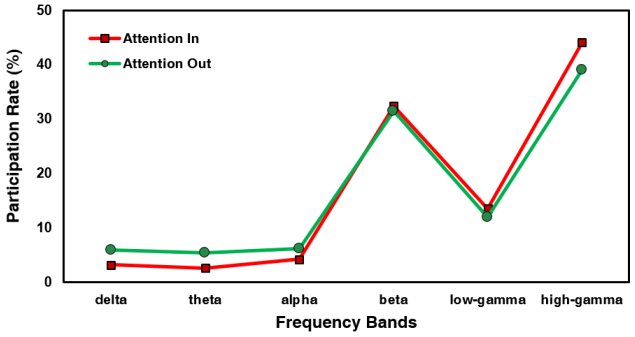

FIGURE 9. The plot depicts the participation ratio of the different frequency bands in motion direction decoding. The participation ratio in the frequency range of 1-120 Hz was calculated according to the repetition of features regarding each frequency sub-band (from among 1736 selected features for attention inside and 2440 selected features for attention outside the RF).

Noticeably, with the number of optimally selected features, the average decoding performance across 28 direction pairs for the target position inside the RF was significantly higher, compared to the target position outside the RF (inside the RF: 90.85% ± 2 (SD) & outside the RF: 86.26% ± 1.8 (SD), $p \ll 0.0001$, two-sided Wilcoxon rank-sum test) (Fig. 8).

E. THE CONTRIBUTION OF FREQUENCY SUB-BANDS TO SELECT INFORMATIVE FEATURE

The optimally selected features were evaluated for determining frequency bands containing informative features in decoding motion direction. Thus, according to the optimum number of features, a total of 1736 features and 2240 features were obtained across 28 directions pairs for inside and outside the RF, respectively. The participation ratio of each frequency band in the classification, based on the number of selected features, demonstrates that the gamma band had the highest contribution out of all frequency bands in decoding motion direction (Fig. 9). This is consistent with the study's previous observations, which showed the high direction-related information content of the gamma band in decoding performance (Fig. 4).

IV. DISCUSSION

This study investigated whether it was possible to decode target motion direction with reliable performance by using LFP recorded from the MT visual cortex. For this purpose, the animal had to attend to the target stimulus, which was moved in one of the possible eight directions (0–360° with steps of 45°), placed inside or outside the RF during the target change-detection task. The outcomes indicated that the mean difference of LFP-power in the high-gamma band for all 28 pairs of motion direction was stronger, compared with those observed in lower frequency ranges (Fig. 2). In agreement with the present results, previous findings have reported LFP gamma-power modulation during the motion direction detection task [28]. It was also found that, as the angular difference between the direction pairs increases, the magnitude of these differences in the high-gamma band also enhances (Fig. 3).

In the next step, the motion direction over a wide range of frequencies was decoded utilizing LFP-power, where the best performance across frequency bands was obtained in the high- gamma band in both spatial attention conditions (Fig. 4). It demonstrated that high-gamma power provides valuable information regarding the prediction of motion direction. Previous studies have demonstrated gamma-band synchronization with spatial and feature attention during visual processing [26], [27], [38], [65], [66]. Additionally, the functional role of high-frequency oscillations has been reported in the allocation of attention decoding [58], [62], spatial attention decoding [57] in the visual cortex area, and also in performance enhancement of movement directions decoding in the motor cortex [49], [50]. The significant performance of the high-gamma band might be due to the high correlation between LFP and spike responses, in terms of direction tuning across visual attention [28], [67]. In line with this hypothesis, several studies have reported functional connections between these neurophysiological signals in different cortical areas [27], [58], [68], [69].

The present study's observation further reveals that when attention is directed toward a stimulus located inside the RF, the classification accuracy in the high-gamma band is significantly higher than when the stimulus is located outside the RF, suggesting spatial attention efficacy on motion direction decoding in the visual system. This observation is in accordance with previous studies indicating that decoding the matching status of two directions from the spike activity was affected by the position of spatial attention in the lateral intraparietal area [46]. Supporting this finding, previous investigations have described similar observations concerning the impact of spatial attention on perceptual performance

during the process of directing attention into the neurons' RF [35]–[37], and the attention-dependent modulation of gamma frequency LFPs in the visual cortical areas [26]–[29].

Along with the above deductions, the present results also illustrated that performance tended to increase in relation to the increasing angular difference of direction pairs, so that decoding performance was best for two targets with 180°-discrepancies (Fig. 5). This is congruent with other studies reporting the dependence of discriminating angular separations on directions differences using the single-unit activity of MT area neurons [70].

The comparison of performances based on temporal windows of different lengths in high-gamma frequency allowed the inference to be made that using longer analysis windows results in an increase in information content and, consequently, an improvement of decoding performance. Thus, decoding accuracy is maximal within analysis windows of 1000 ms width in both attention conditions (Fig. 7). Furthermore, attentional information is most apparent in the time interval starting from 200 ms after the onset of target presentation.

In the current study, it was derived that using optimally selected features leads to improvements in the decoding performance of motion direction in visual attention (Fig. 8). It was observed that the gamma band contains the highest proportion of these features, compared to other frequency bands, in target direction decoding (Fig. 9). This indicates the high information content in the gamma band, which is compatible with attentional modulation observations in this frequency range [26]–[28].

V. CONCLUSION

This study demonstrated the ability for reliably decoding motion direction using LFP signals from the MT area of the macaque visual cortex during spatial-based attention task. It was found that the best performance was achieved in gamma-frequency oscillations, which reflected a high level of coded attentional information in this frequency range. Importantly, the results indicated the influence of spatial attention on target direction decoding, so that directing attention inside the RF was correlated with improved performance. Overall, these findings suggest that the visual information of LFP signals can be utilized for developing cognitive BCI systems.

ACKNOWLEDGMENT

The authors wish to thank Dr. Stefan Treue and the German Primate Center–Leibniz Institute for Primate Research (DPZ) to provide the infrastructure and intellectual support for recording the data.

REFERENCES

[1] M. Carrasco, "Visual attention: The past 25 years," *Vis. Res.*, vol. 51, no. 13, pp. 1484–1525, Jul. 2011.

[2] M. R. Cohen and J. H. R. Maunsell, "Using neuronal populations to study the mechanisms underlying spatial and feature attention," *Neuron*, vol. 70, no. 6, pp. 1192–1204, Jun. 2011.

[3] J. Ekanayake, C. Hutton, G. Ridgway, F. Scharnowski, N. Weiskopf, and G. Rees, "Real-time decoding of covert attention in higher-order visual areas," *NeuroImage*, vol. 169, pp. 462–472, Apr. 2018.

[4] A. Ahmadi, S. Davoudi, M. Behroozi, and M. R. Daliri, "Decoding covert visual attention based on phase transfer entropy," *Physiol. Behav.*, vol. 222, Aug. 2020, Art. no. 112932.

[5] D. Kim, W. Byun, Y. Ku, and J.-H. Kim, "High-speed visual target identification for low-cost wearable brain-computer interfaces," *IEEE Access*, vol. 7, pp. 55169–55179, Apr. 2019.

[6] K.-T. Kim, J. Lee, H. Kim, C. H. Kim, and S. J. Lee, "Classification of selective attention within steady-state somatosensory evoked potentials from dry electrodes using mutual information-based spatio-spectral feature selection," *IEEE Access*, vol. 8, pp. 85464–85472, Apr. 2020.

[7] A. Gaume, G. Dreyfus, and F.-B. Vialatte, "A cognitive brain–computer interface monitoring sustained attentional variations during a continuous task," *Cogn. Neurodyn.*, vol. 13, no. 3, pp. 257–269, Jun. 2019.

[8] A. Tankus, I. Fried, and S. Shoham, "Cognitive-motor brain–machine interfaces," *J. Physiol.-Paris*, vol. 108, no. 1, pp. 38–44, Feb. 2014.

[9] M. R. Daliri, "A hybrid method for the decoding of spatial attention using the MEG brain signals," *Biomed. Signal Process. Control*, vol. 10, pp. 308–312, Mar. 2014.

[10] D. Zhang, A. Maye, X. Gao, B. Hong, A. K. Engel, and S. Gao, "An independent brain–computer interface using covert non-spatial visual selective attention," *J. Neural Eng.*, vol. 7, no. 1, Jan. 2010, Art. no. 016010.

[11] L. Tonin, R. Leeb, A. Sobolewski, and J. D. R. Millán, "An online EEG BCI based on covert visuospatial attention in absence of exogenous stimulation," *J. Neural Eng.*, vol. 10, no. 5, Aug. 2013, Art. no. 056007.

[12] Z. Oralhan, "A new paradigm for region-based P300 speller in brain computer interface," *IEEE Access*, vol. 7, pp. 106618–106627, Aug. 2019.

[13] Z. Oralhan, "3D input convolutional neural networks for P300 signal detection," *IEEE Access*, vol. 8, pp. 19521–19529, Jan. 2020.

[14] C. J. Ortiz-Echeverri, S. Salazar-Colores, J. Rodríguez-Reséndiz, and R. A. Gómez-Loenzo, "A new approach for motor imagery classification based on sorted blind source separation, continuous wavelet transform, and convolutional neural network," *Sensors*, vol. 19, no. 20, p. 4541, Oct. 2019.

[15] T. Milekovic, A. A. Sarma, D. Bacher, J. D. Simeral, J. Saab, C. Pandarinath, B. L. Sorice, C. Blabe, E. M. Oakley, K. R. Tringale, E. Eskandar, S. S. Cash, J. M. Henderson, K. V. Shenoy, J. P. Donoghue, and L. R. Hochberg, "Stable long-term BCI-enabled communication in ALS and locked-in syndrome using LFP signals," *J. Neurophysiol.*, vol. 120, no. 1, pp. 343–360, Jul. 2018.

[16] J. A. Perge, S. Zhang, W. Q. Malik, M. L. Homer, S. Cash, G. Friehs, E. N. Eskandar, J. P. Donoghue, and L. R. Hochberg, "Reliability of directional information in unsorted spikes and local field potentials recorded in human motor cortex," *J. Neural Eng.*, vol. 11, no. 4, Jun. 2014, Art. no. 046007.

[17] N. Ahmadi, T. G. Constandinou, and C.-S. Bouganis, "Impact of referencing scheme on decoding performance of LFP-based brain-machine interface," *J. Neural Eng.*, vol. 18, no. 1, Feb. 2021, Art. no. 016028.

[18] G. Buzsáki, C. A. Anastassiou, and C. Koch, "The origin of extracellular fields and currents—EEG, ECoG, LFP and spikes," *Nature Rev. Neurosci.*, vol. 13, no. 6, pp. 407–420, Jun. 2012.

[19] J. D. Simeral, S.-P. Kim, M. J. Black, J. P. Donoghue, and L. R. Hochberg, "Neural control of cursor trajectory and click by a human with tetraplegia 1000 days after implant of an intracortical microelectrode array," *J. Neural Eng.*, vol. 8, no. 2, Mar. 2011, Art. no. 025027.

[20] J. A. Perge, M. L. Homer, W. Q. Malik, S. Cash, E. Eskandar, G. Friehs, J. P. Donoghue, and L. R. Hochberg, "Intra-day signal instabilities affect decoding performance in an intracortical neural interface system," *J. Neural Eng.*, vol. 10, no. 3, Apr. 2013, Art. no. 036004.

[21] J. C. Barrese, N. Rao, K. Paroo, C. Triebwasser, C. Vargas-Irwin, L. Franquemont, and J. P. Donoghue, "Failure mode analysis of silicon-based intracortical microelectrode arrays in non-human primates," *J. Neural Eng.*, vol. 10, no. 6, Nov. 2013, Art. no. 066014.

[22] A. Jackson and T. M. Hall, "Decoding local field potentials for neural interfaces," *IEEE Trans. Neural Syst. Rehabil. Eng.*, vol. 25, no. 10, pp. 1705–1714, Oct. 2017.

[23] S. D. Stavisky, J. C. Kao, P. Nuyujukian, S. I. Ryu, and K. V. Shenoy, "A high performing brain–machine interface driven by low-frequency local field potentials alone and together with spikes," *J. Neural Eng.*, vol. 12, no. 3, May 2015, Art. no. 036009.

[24] R. D. Flint, M. R. Scheid, Z. A. Wright, S. A. Solla, and M. W. Slutzky, "Long-term stability of motor cortical activity: Implications for brain machine interfaces and optimal feedback control," *J. Neurosci.*, vol. 36, no. 12, pp. 3623–3632, Mar. 2016.
[25] J. W. Bisley, "The neural basis of visual attention," *J. Physiol.*, vol. 589, no. 1, pp. 49–57, Jan. 2011.
[26] P. Fries, "Modulation of oscillatory neuronal synchronization by selective visual attention," *Science*, vol. 291, no. 5508, pp. 1560–1563, Feb. 2001.
[27] P. Fries, T. Womelsdorf, R. Oostenveld, and R. Desimone, "The effects of visual stimulation and selective visual attention on rhythmic neuronal synchronization in macaque area V4," *J. Neurosci.*, vol. 28, no. 18, pp. 4823–4835, Apr. 2008.
[28] P. S. Khayat, R. Niebergall, and J. C. Martinez-Trujillo, "Frequency-dependent attentional modulation of local field potential signals in macaque area MT," *J. Neurosci.*, vol. 30, no. 20, pp. 7037–7048, May 2010.
[29] M. Chalk, J. L. Herrero, M. A. Gieselmann, L. S. Delicato, S. Gotthardt, and A. Thiele, "Attention reduces stimulus-driven gamma frequency oscillations and spike field coherence in V1," *Neuron*, vol. 66, no. 1, pp. 114–125, Apr. 2010.
[30] M. Vinck, T. Womelsdorf, E. A. Buffalo, R. Desimone, and P. Fries, "Attentional modulation of cell-class-specific gamma-band synchronization in awake monkey area V4," *Neuron*, vol. 80, no. 4, pp. 1077–1089, Nov. 2013.
[31] X. Chen, K.-P. Hoffmann, T. D. Albright, and A. Thiele, "Effect of feature-selective attention on neuronal responses in macaque area MT," *J. Neurophysiol.*, vol. 107, no. 5, pp. 1530–1543, Mar. 2012.
[32] B. Schledde, F. O. Galashan, M. Przybyla, A. K. Kreiter, and D. Wegener, "Task-specific, dimension-based attentional shaping of motion processing in monkey area MT," *J. Neurophysiol.*, vol. 118, no. 3, pp. 1542–1555, Sep. 2017.
[33] V. Kozyrev, M. R. Daliri, P. Schwedhelm, and S. Treue, "Strategic deployment of feature-based attentional gain in primate visual cortex," *PLOS Biol.*, vol. 17, no. 8, Aug. 2019, Art. no. e3000387.
[34] J. R. Hembrook-Short, V. L. Mock, and F. Briggs, "Attentional modulation of neuronal activity depends on neuronal feature selectivity," *Current Biol.*, vol. 27, no. 13, pp. 1878–1887, Jul. 2017.
[35] J. H. Reynolds and D. J. Heeger, "The normalization model of attention," *Neuron*, vol. 61, no. 2, pp. 168–185, Jan. 2009.
[36] K. A. Sundberg, J. F. Mitchell, and J. H. Reynolds, "Spatial attention modulates center-surround interactions in macaque visual area V4," *Neuron*, vol. 61, no. 6, pp. 952–963, Mar. 2009.
[37] S. Treue and J. H. R. Maunsell, "Effects of attention on the processing of motion in macaque middle temporal and medial superior temporal visual cortical areas," *J. Neurosci.*, vol. 19, no. 17, pp. 7591–7602, Sep. 1999.
[38] E. A. Buffalo, P. Fries, R. Landman, T. J. Buschman, and R. Desimone, "Laminar differences in gamma and alpha coherence in the ventral stream," *Proc. Nat. Acad. Sci. USA*, vol. 108, no. 27, pp. 11262–11267, Jul. 2011.
[39] J. H. R. Maunsell and S. Treue, "Feature-based attention in visual cortex," *Trends Neurosci.*, vol. 29, no. 6, pp. 317–322, Jun. 2006.
[40] J. C. Martinez-Trujillo and S. Treue, "Feature-based attention increases the selectivity of population responses in primate visual cortex," *Current Biol.*, vol. 14, no. 9, pp. 744–751, May 2004.
[41] S. Treue and J. C. M. Trujillo, "Feature-based attention influences motion processing gain in macaque visual cortex," *Nature*, vol. 399, no. 6736, pp. 575–579, Jun. 1999.
[42] P. M. Kaskan, B. C. Dillenburger, H. D. Lu, and A. W. Roe, "Orientation and direction-of-motion response in the middle temporal visual area (MT) of New World owl monkeys as revealed by intrinsic-signal optical imaging," *Frontiers Neuroanatomy*, vol. 4, p. 23, Jul. 2010.
[43] C. J. McAdams and J. H. R. Maunsell, "Attention to both space and feature modulates neuronal responses in macaque area V4," *J. Neurophysiol.*, vol. 83, no. 3, pp. 1751–1755, Mar. 2000.
[44] S. Katzner, L. Busse, and S. Treue, "Attention to the color of a moving stimulus modulates motion-signal processing in macaque area MT: Evidence for a unified attentional system," *Frontiers Syst. Neurosci.*, vol. 3, p. 12, Oct. 2009.
[45] G. Liang and M. Scolari, "Limited interactions between space-and feature-based attention in visually sparse displays," *J. Vis.*, vol. 20, no. 4, p. 5, Apr. 2020.
[46] G. Ibos and D. J. Freedman, "Interaction between spatial and feature attention in posterior parietal cortex," *Neuron*, vol. 91, no. 4, pp. 931–943, Aug. 2016.
[47] B. Y. Hayden and J. L. Gallant, "Combined effects of spatial and feature-based attention on responses of V4 neurons," *Vis. Res.*, vol. 49, no. 10, pp. 1182–1187, Jun. 2009.
[48] D. R. Patzwahl and S. Treue, "Combining spatial and feature-based attention within the receptive field of MT neurons," *Vis. Res.*, vol. 49, no. 10, pp. 1188–1193, Jun. 2009.
[49] N. F. Ince, R. Gupta, S. Arica, A. H. Tewfik, J. Ashe, and G. Pellizzer, "High accuracy decoding of movement target direction in non-human primates based on common spatial patterns of local field potentials," *PLoS ONE*, vol. 5, no. 12, Dec. 2010, Art. no. e14384.
[50] R. D. Flint, E. W. Lindberg, L. R. Jordan, L. E. Miller, and M. W. Slutzky, "Accurate decoding of reaching movements from field potentials in the absence of spikes," *J. Neural Eng.*, vol. 9, no. 4, Jun. 2012, Art. no. 046006.
[51] D. Wang, Q. Zhang, Y. Li, Y. Wang, J. Zhu, S. Zhang, and X. Zheng, "Long-term decoding stability of local field potentials from silicon arrays in primate motor cortex during a 2D center out task," *J. Neural Eng.*, vol. 11, no. 3, May 2014, Art. no. 036009.
[52] M. W. Slutzky, L. R. Jordan, E. W. Lindberg, K. E. Lindsay, and L. E. Miller, "Decoding the rat forelimb movement direction from epidural and intracortical field potentials," *J. Neural Eng.*, vol. 8, no. 3, Apr. 2011, Art. no. 036013.
[53] P. Zhang, J. Huang, W. Li, X. Ma, P. Yang, J. Dai, and J. He, "Using high-frequency local field potentials from multicortex to decode reaching and grasping movements in monkey," *IEEE Trans. Cognit. Develop. Syst.*, vol. 11, no. 2, pp. 270–280, Jun. 2019.
[54] D. A. E. Kaliukhovich and R. Vogels, "Decoding of repeated objects from local field potentials in macaque inferior temporal cortex," *PLoS ONE*, vol. 8, no. 9, Sep. 2013, Art. no. e74665.
[55] Y. Zhang, E. M. Meyers, N. P. Bichot, T. Serre, T. A. Poggio, and R. Desimone, "Object decoding with attention in inferior temporal cortex," *Proc. Nat. Acad. Sci. USA*, vol. 108, no. 21, pp. 8850–8855, May 2011.
[56] M. Esghaei and M. R. Daliri, "Decoding of visual attention from LFP signals of macaque MT," *PLoS ONE*, vol. 9, no. 6, Jun. 2014, Art. no. e100381.
[57] Z. Seif and M. R. Daliri, "Evaluation of local field potential signals in decoding of visual attention," *Cognit. Neurodyn.*, vol. 9, no. 5, pp. 509–522, Oct. 2015.
[58] S. Tremblay, G. Doucet, F. Pieper, A. Sachs, and J. Martinez-Trujillo, "Single-trial decoding of visual attention from local field potentials in the primate lateral prefrontal cortex is frequency-dependent," *J. Neurosci.*, vol. 35, no. 24, pp. 9038–9049, Jun. 2015.
[59] S. Tremblay, F. Pieper, A. Sachs, and J. Martinez-Trujillo, "Attentional filtering of visual information by neuronal ensembles in the primate lateral prefrontal cortex," *Neuron*, vol. 85, no. 1, pp. 202–215, Jan. 2015.
[60] L. Duong, M. Leavitt, F. Pieper, A. Sachs, and J. Martinez-Trujillo, "A normalization circuit underlying coding of spatial attention in primate lateral prefrontal cortex," *Eneuro*, vol. 6, no. 2, Mar. 2019.
[61] E. Astrand, C. Wardak, P. Baraduc, and S. Ben Hamed, "Direct two-dimensional access to the spatial location of covert attention in macaque prefrontal cortex," *Current Biol.*, vol. 26, no. 13, pp. 1699–1704, Jul. 2016.
[62] D. Rotermund, U. A. Ernst, S. Mandon, K. Taylor, Y. Smiyukha, A. K. Kreiter, and K. R. Pawelzik, "Toward high performance, weakly invasive brain computer interfaces using selective visual attention," *J. Neurosci.*, vol. 33, no. 14, pp. 6001–6011, Apr. 2013.
[63] C. Cortes and V. Vapnik, "Support-vector networks," *Mach. Learn.*, vol. 20, no. 3, pp. 273–297, Sep. 1995.
[64] P. Zarei Eskikand, T. Kameneva, A. N. Burkitt, D. B. Grayden, and M. R. Ibbotson, "Pattern motion processing by MT neurons," *Frontiers Neural Circuits*, vol. 13, p. 43, Jun. 2019.
[65] K. Taylor, S. Mandon, W. A. Freiwald, and A. K. Kreiter, "Coherent oscillatory activity in monkey area V4 predicts successful allocation of attention," *Cerebral Cortex*, vol. 15, no. 9, pp. 1424–1437, Sep. 2005.
[66] G. G. Gregoriou, S. J. Gotts, H. Zhou, and R. Desimone, "High-frequency, long-range coupling between prefrontal and visual cortex during attention," *Science*, vol. 324, no. 5931, pp. 1207–1210, May 2009.
[67] J. Liu and W. T. Newsome, "Local field potential in cortical area MT: Stimulus tuning and behavioral correlations," *J. Neurosci.*, vol. 26, no. 30, pp. 7779–7790, Jul. 2006.
[68] S. Ray and J. H. R. Maunsell, "Different origins of gamma rhythm and high-gamma activity in macaque visual cortex," *PLoS Biol.*, vol. 9, no. 4, Apr. 2011, Art. no. e1000610.

[69] D. Xing, C.-I. Yeh, and R. M. Shapley, "Spatial spread of the local field potential and its laminar variation in visual cortex," *J. Neurosci.*, vol. 29, no. 37, pp. 11540–11549, Sep. 2009.
[70] J. S. McDonald, C. W. G. Clifford, S. S. Solomon, S. C. Chen, and S. G. Solomon, "Integration and segregation of multiple motion signals by neurons in area MT of primate," *J. Neurophysiol.*, vol. 111, no. 2, pp. 369–378, Jan. 2014.

MOHAMMAD REZA NAZARI received the B.Sc. degree in electrical engineering from the Shahid Bahonar University of Kerman, Kerman, Iran, in 2006, and the M.Sc. degree in biomedical engineering from the Khajeh Nasir Toosi University of Technology, Tehran, Iran, in 2009. He is currently pursuing the Ph.D. degree in biomedical engineering with Islamic Azad University, Science and Research Branch. He has been a Faculty Member with the Department of Biomedical Engineering, Qazvin Islamic Azad University, since 2010. His current research interests include biomedical signal processing, brain–computer interfaces, and cognitive neuroscience.

ALI MOTIE NASRABADI received the B.Sc. degree in electronic engineering and the M.Sc. and Ph.D. degrees in biomedical engineering from the Amirkabir University of Technology, Tehran, Iran, in 1994, 1999, and 2004, respectively. In 2004, he joined the Biomedical Engineering Department, Faculty of Engineering, Shahed University, where he was an Assistant Professor, from 2004 to 2011, an Associate Professor, from 2011 to 2017, and has been a Full Professor, since 2017. He is currently a Scientific Advisor with the National Brain Mapping Laboratory, University of Tehran, Iran. His current research interests include brain–computer interfaces, biomedical signal processing, machine learning, deep learning, nonlinear time series analysis, and computational neuroscience. He is a Board Member of the Iranian Society for Biomedical Engineering and has served on the scientific committees for several national conferences and review boards of five scientific journals.

MOHAMMAD REZA DALIRI (Member, IEEE) received the M.Sc. degree in medical radiation engineering from the Amirkabir University of Technology, Tehran, Iran, in 2001, and the Ph.D. degree in cognitive neuroscience from the International School for Advanced Studies (SISSA/ISAS), Trieste, Italy, in 2007. From 2007 to 2009, he was a Postdoctoral Fellow with SISSA/ISAS, and the German Primate Center (DPZ), Göttingen, Germany. He is currently a Full Professor with the Department of Biomedical Engineering, School of Electrical Engineering, Iran University of Science and Technology (IUST), Tehran. His main research interests include neural signal processing, brain–computer interfaces, computational and cognitive neuroscience, pattern recognition, and computer vision.